Key Points:
- Data from the Langmuir Probe and Waves instrument reveal density structures in the Mars ionosphere
- MAVEN samples an altitude range which previously has only been sparsely explored in situ
- MAVEN/LPW data also reveal the stabilizing influence of intense crustal fields

Correspondence to:
D. J. Andrews,
david.andrews@irfu.se

Ionospheric plasma density variations observed at Mars by MAVEN/LPW

D. J. Andrews[1], L. Andersson[2], G. T. Delory[3], R. E. Ergun[2], A. I. Eriksson[1], C. M. Fowler[2], T. McEnulty[2], M. W. Morooka[2], T. Weber[2], and B. M. Jakosky[2]

[1]Swedish Institute of Space Physics (Uppsala), Uppsala, Sweden, [2]Laboratory of Atmospheric and Space Physics, ,Boulder, Colorado, USA, [3]Space Sciences Laboratory, University of California, Berkeley, USA

Abstract We report on initial observations made by the Langmuir Probe and Waves relaxation sounding experiment on board the NASA Mars Atmosphere and Volatile EvolutioN (MAVEN) mission. These measurements yield the ionospheric thermal plasma density, and we use these data here for an initial survey of its variability. Studying orbit-to-orbit variations, we show that the relative variability of the ionospheric plasma density is lowest at low altitudes near the photochemical peak, steadily increases toward higher altitudes and sharply increases as the spacecraft crosses the terminator and moves into the nightside. Finally, despite the small volume of data currently available, we show that a clear signature of the influence of crustal magnetic fields on the thermal plasma density fluctuations is visible. Such results are consistent with previously reported remote measurements made at higher altitudes, but crucially, here we sample a new span of altitudes between ∼130 and ∼300 km using in situ techniques.

1. Introduction

The plasma density structure of the Martian ionosphere has been studied in detail through both remote and in situ measurement techniques across several decades. Profiles obtained during the descents of the Viking landers [*Hanson et al.*, 1977] have been supplemented by extensive sets of data obtained through radio occultation [e.g., *Pätzold et al.*, 2004; *Tyler et al.*, 2001], charged particle detectors [e.g., *Mitchell et al.*, 2001; *Barabash et al.*, 2006], and topside radio sounding [*Picardi et al.*, 2004; *Gurnett et al.*, 2005]. Collectively, these measurements reveal the presence of a dayside ionosphere, with peak densities reaching ∼1.5×10^5 cm^{-3} at altitudes of ∼125 km, which is in photochemical equilibrium at these altitudes with recombination as the dominant loss process [see, e.g., *Nagy et al.*, 2004; *Witasse et al.*, 2008; *Withers*, 2009, and references therein]. Beyond the terminator the plasma density drops rapidly, and only localized regions of sporadically produced plasma are observed, which may originate either in transterminator flows from the dayside or production through energetic particle precipitation [e.g., *Němec et al.*, 2010, 2011a; *Fowler et al.*, 2015]. Furthermore, Mars's spatially varying crustal magnetic fields are in places intense enough to dominate over externally draped solar wind magnetic fields, and thereby effect changes in the transport of ionospheric plasma [*Acuña et al.*, 1998; *Cain et al.*, 2003].

In this paper we report on initial observations made using data from the Langmuir Probe and Waves (LPW) instrument on Mars Atmosphere and Volatile EvolutioN (MAVEN) mission. LPW consists of two cylindrical ∼40×0.6 cm Langmuir probes mounted on 7 m booms, deployed following its arrival at Mars on 22 September 2014 UTC. Full details of the instrument design and operation are provided by *Andersson et al.* [2015]. The instrument design includes elements from somewhat similar experiments flown on Thermal Emission Imaging System, FAST, and Polar. The two probes can be operated independently. Operated as Langmuir probes, conduct current-voltage (*I-V*) sweeps are performed from which the electron density and temperature can be derived, among other parameters of the plasma. Initial results from this mode of operation are presented in companion papers in this issue [*Ergun et al.*, 2015; *Fowler et al.*, 2015], in which dayside profiles of ionospheric density and temperature, and properties of the nightside ionosphere are respectively described. Alternatively, the probes can be operated as electric field sensors, measuring one component of the field at frequencies from ∼1 to 2×10^6 Hz, and we focus on the results from this mode of operation in this paper. The operation of the probes follows a fixed master cycle sequence, consisting of two *I-V* sweeps (one on each probe), interspersed with two electric field measurement intervals, in which one

is "passive" and one "active". During both passive and active measurements, spectra are computed from the measured fields by processing electronics on board the spacecraft. In the passive mode, any naturally occurring plasma waves will be detected, the most intense of which we expect to be at the local plasma frequency f_{pe}. Meanwhile, in the active mode a brief ∼15 ms white noise sounding pulse is transmitted on the LPW booms, and immediately following this, any stimulated natural plasma emissions are measured. The principal aim of this active experiment is in yielding a measurable amplitude of the plasma waves across a larger fraction of each orbit, in practice allowing the determination of the local plasma density n_e from the local electron plasma frequency at lower densities than is possible in passive mode in the upper ionosphere. We remind the reader of the relationship $f_{pe} \approx 8980 n_e^{1/2}$ where f_{pe} is in hertz and n_e is in cm^{-3}. Thus, the active mode, also termed "relaxation sounding" or "pinging" can provide a reliable lower density bound to values derived from the *I-V* sweeps also performed by LPW. Measurable local plasma waves are only infrequently observed in the passive operation mode, while the routine operation of the active mode was only commenced from 8 January 2015 onward. Through having multiple techniques by which the thermal electron density can be obtained, intercalibration can be performed revealing the impact of changing spacecraft-plasma interactions and possible variations in the sensor characteristics.

In addition to LPW, MAVEN comprises a comprehensive suite of sensors relevant to the study of the Martian ionosphere [*Jakosky et al.*, 2015]. The elliptical orbit of the spacecraft is 150 × 6200 km, at an inclination of ∼75°, with periapsis being temporarily lowered to ∼130 km during several so-called "deep-dips", each lasting ∼5 days.

In this paper we focus our analysis on the characterization of density fluctuations in the Martian ionosphere, as wave mode measurements available from LPW can reveal variations in density to exceptionally high accuracy. Recent studies of variations in the ionospheric plasma density at Mars have chiefly been conducted using both in situ and remote-sounding measurements made by the Mars Advanced Radar for Sub-Surface and Ionospheric Sounding (MARSIS) onboard ESA's Mars Express (MEX) spacecraft. For example, *Gurnett et al.* [2010] have shown that density fluctuations with spectral variations typical of Alfvénic turbulence are present throughout the Martian ionosphere, though it remains unclear whether such fluctuations are imposed upon the plasma by motions of the upper boundary, the upward propagation of breaking gravity waves, or some other mechanism. Relative to the dayside, the nightside ionosphere is generally less extensively studied, but it is nevertheless well known that localized patches of ionization are often found, in particular over regions where the Martian crustal field may control the precipitation of ionizing electrons [e.g., *Duru et al.*, 2011; *Lillis et al.*, 2009; *Lillis and Brain*, 2013; *Němec et al.*, 2010, 2011b, 2014]. The spatially and temporally varied nature of the Martian near-terminator ionosphere is also seen in radio occultation measurements, as shown, e.g., by *Zhang et al.* [1990] and *Kliore* [1992], but geometrical considerations make it impossible to observe the deep nightside.

One of Mars's unique aspects is its spatially localized and highly varied crustal magnetic fields [*Acuña et al.*, 1998], which are in certain places of sufficient strength as to exceed typical draped solar wind field strengths on the dayside [e.g., *Brain et al.*, 2003]. The Martian crustal fields have also been shown to influence the configuration of the ionosphere, at altitudes well above the peak, in large statistical surveys [*Lundin et al.*, 2011; *Nilsson et al.*, 2011; *Dubinin et al.*, 2012; *Andrews et al.*, 2013, 2015]. This likely goes some way to explaining the observed variability of plasma boundaries such as the transient sharp gradient in plasma density at the so-called "ionopause," or the increase in the draped field strength at the magnetic pile-up boundary, and their respective dependence on the crustal fields [e.g., *Brain et al.*, 2005; *Duru et al.*, 2009; *Edberg et al.*, 2008]. Furthermore, stable small-scale structures in the ionosphere have been regularly observed in remote sounding measurements [*Gurnett et al.*, 2005; *Duru et al.*, 2006; *Andrews et al.*, 2014] in regions of near-radial "cusp-like" magnetic fields, at lower altitudes closer to the ionospheric peak. Measurements made using the subsurface sounding mode of MARSIS have also revealed a close correlation between ionospheric total electron content (integrated column density) and crustal field orientation [*Cartacci et al.*, 2013; *Mendillo et al.*, 2013]. In situ measurements made by MAVEN at ionospheric altitudes provide an opportunity to study some of these processes in more detail as follows.

2. Observations

In Figure 1 we show examples of LPW data and MAVEN positional information obtained surrounding the periapsis of orbit 782 on 24 February 2015, at ∼03:50 Coordinated Universal Time (UTC, as for all time instances
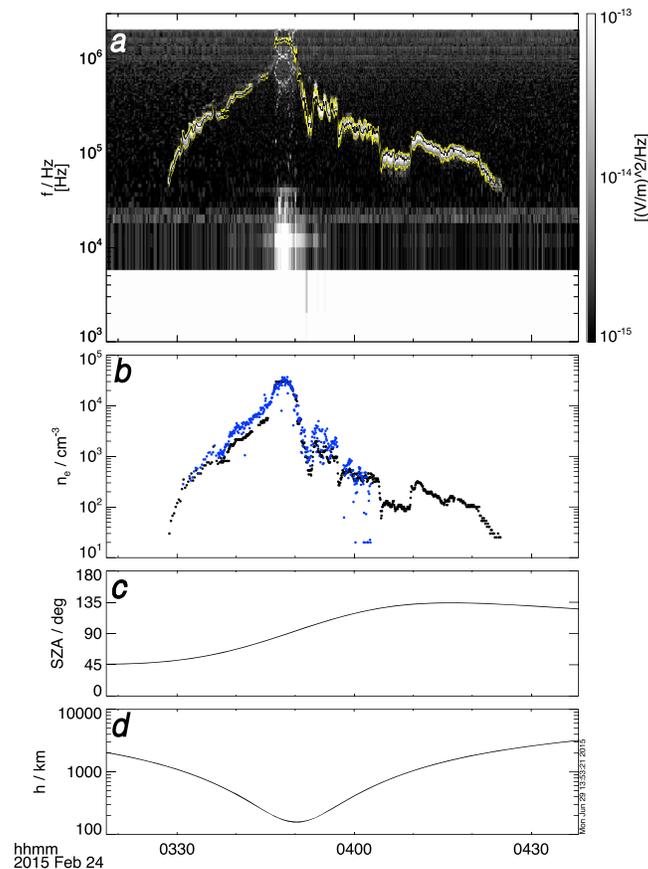
Figure 1. MAVEN LPW high-frequency relaxation sounding data. (a) On board calculated electric field wave spectra, with black and yellow lines overplotted showing the peak determined wave power, and the upper and lower bounds of the spectral feature, respectively. (b) The inferred electron plasma density from the relaxation sounding (black circles) and the current-voltage sweeps (blue circles). (c and d) The SZA and altitude of MAVEN, respectively.

given hereafter). Figure 1a shows the *E* field spectral density obtained following the transmission of the white noise relaxation sounding pulse, once per master cycle (i.e., every 4 s at the highest rate). From 03:27 to 04:25 a clear spectral peak is present in these data which rises to a peak at periapsis before falling again on the outbound leg. The frequency of the most intense feature in the spectra is indicated by the black line in Figure 1b, converted to a plasma density value, with the bounding yellow lines indicting the width of the peak before it diminishes to background values. For comparison purposes, electron densities derived from the current-voltage (*I-V*) sweeps also performed by LPW during this period are shown by the blue points in Figure 1c, along with the solar zenith angle (SZA) in Figure 1d and altitude in Figure 1e.

The reader will note that these two independent measurements of plasma density begin to deviate from one another as the density recorded by the active sounding rises above $\sim 10^3$ cm^{-3}, possibly due to the formation of a localized electron density cavity around the spacecraft and its various sensors and consequent trapping of the eigenmode(s) of a Langmuir oscillation within it [e.g., *Ergun et al.*, 2008; *Ergun et al.*, 2015; *Fowler et al.*, 2015]. A sudden apparent jump in density is then recorded by the active measurements at ~03:46, and the waves-derived densities again reaches values that are in broad agreement with that obtained from the *I-V* sweeps. This apparent jump occurs at the same time the peak spectral power rises, by several orders of magnitude, and additional nonphysical spectral lines become clear in the data, along with a large increase in the wave power at low frequencies below $\sim 3 \times 10^4$ Hz. All these changes occur with no apparent coincident sharp variation in the character of the *I-V* sweep data themselves, as shown in a logarithmic scale in Figure 1c. We conclude that these changes in the wave spectra are instead the result of self-excited oscillations in the probe-plasma circuit, resonant at f_{pe}, causing both the large increase in the measured amplitude of the waves, clipping and/or mixing of these waves with characteristic instrumental frequencies, and a change in the probe potential caused by partial rectification of these waves owing to the nonlinear current-voltage

relationship [e.g., *Boehm et al.*, 1994; *Kolesnikova et al.*, 2001]. Owing to the large amplitude feedback at the plasma frequency, we expect that these nevertheless represent accurate measurements of the local plasma density, despite the otherwise somewhat degraded spectra obtained in this regime. The instrument exits this condition of self-oscillation following periapsis as the density drops at $\sim$03:51, and once again the density reported by the active sounding is significantly lower than that from the *I-V* sweeps until the density has fallen to values once again below $\sim 10^3$ cm^{-3}.

In summary, our interpretation of these data is that several distinct regimes exist, characterized by the Debye lengths λ_D and approximate densities n_e, as follows: (a) $\lambda_D > 1$ m ($n_e < 10^3$ cm^{-3}), such that no significant density cavity forms around the spacecraft, and the measured wave frequency accurately reflects the unperturbed plasma frequency; (b) 1 m $> \lambda_D > 1$ cm (10^3 cm$^{-3} < n_e < 10^4$ cm^{-3}), such that a significant density cavity forms and grows in depth about the spacecraft and antennas, and the measured plasma frequency instead reflects a natural mode of the cavity; and (c) $\lambda_D < 1$ cm ($n_e > 10^4$ cm^{-3}), such that a capacitive coupling and positive feedback is established between the sensor and the adjacent stub, driving the instrument into a self-sustained oscillation but in which the density cavity is no longer present or at least significant, and the measured plasma frequency is once again comparable to that of the unperturbed plasma. We note that further development and modeling is required to fully understand the these effects.

With this in mind, in this paper we concentrate on characterizing the orbit-to-orbit variations seen in the Martian ionospheric plasma. Analyses of the plasma density and temperature obtained from *I-V* sweeps by LPW is presented instead in two companion papers in this issue [*Ergun et al.*, 2015; *Fowler et al.*, 2015]. Here we compute a measure of the density variability by time shifting the plasma density recorded on each orbit i, such that periapsis of every orbit occurs at time $t = 0$. This allows us to directly compare the measured along-orbit variation of $n_e(t)$ for orbit i with that obtained from the average of its 2N immediate neighbors $\{i - N, i - N + 1, \ldots, i - 1, i + 1, \ldots, i + N - 1, i + N\}$, which we label n_e^*. In this way, the slow drift of the principal coordinates SZA and h from one periapsis to the next does not strongly contribute to the averaged profile, and instead we can examine other sources of variation. In choosing a value for N, a compromise between capturing the slow variation of the density with SZA and h, and yielding a sufficient sampling of data that the average over the 2N traces is meaningful. Values of N from 1 to 10 were tested, and $N = 2$ was selected for presentation. The results are only weakly sensitive to the value of N, providing that it is not so large that the trajectory of the spacecraft through SZA $\times$ h space changes significantly. A value of $N = 2$ corresponds to the average profile n_e^* being determined over an interval of $\sim$23 h duration. Furthermore, the implicit differencing involved in this technique allows us to mitigate, as much as possible, the effects associated with the changing performance of the waves measurement within each orbit.

An example of this process is shown in Figure 2, for orbit 782. Figure 2a shows the plasma density profiles recorded on the adjacent N orbits (specifically 780 to 784) as grey lines, while that recorded on the orbit in question is shown in black. The corresponding averaged density profile $n_e^*(t)$ is shown in red. Figure 2b then shows the signed deviation between the red and black traces in Figure 2a. Figures 2c and 2d show MAVEN's trajectory at periapsis in SZA and altitude h, respectively, and in each case the grey traces for the adjacent orbits are obscured by that of the central orbit 782 shown in black, indicating only a small difference in these coordinates during periapsis for these 5 orbits.

For the specific example shown in Figure 2, we note several important features. First, on orbit 782 shown by the black trace, no feature resembling the so-called ionopause is observed, and the measured plasma density steadily rises and falls, excepting at that point indicated by the blue vertical bar $\sim$5 min before periapsis, which rather marks the transition into the self-induced oscillation of the instrument. The second blue bar indicates the exit from this operation regime, and we note that within each separate trace shown in this figure, the timing of these transitions does not vary by more than the measurement cadence. Owing to the trajectory of the spacecraft, peak plasma densities are reached on all orbits slightly before periapsis, and the density varies in general more steadily along the orbit on the dayside than is true on the nightside. In contrast to the black trace (orbit 782), large density gradients indicative of crossings of the so-called ionopause are seen the inbound segments of two of the four grey-colored orbits, in each case centered around $\sim$15 min before periapsis. Nondetections of the local plasma oscillation prior to this on these orbits leads to the averaged density variation (red trace) being undefined prior to this.
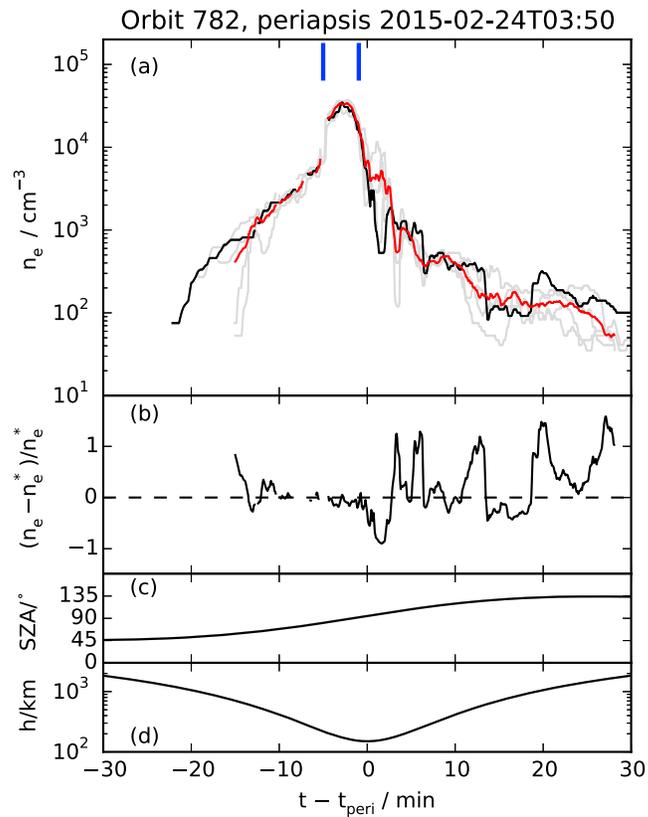
Figure 2. Computed density variations, time shifted according to the periapsis of their respective orbits. (a) n_e derived on orbits 782 (black line) and the two preceding and two following orbits (grey lines). The red line, n_e^*, is the computed average of the four grey traces shown. The vertical blue bars indicates the two apparent density discontinuities induced by the changing coupling between the probe and plasma. (b) The scaled deviation between the black and red traces in Figure 2a. (c and d) The SZA and altitude of each orbit shown in Figure 2a, though we note the small differences in traces do not allow them to be individually resolved.

In Figure 3 we plot the absolute quantity $\Delta n_e/n_e^* = |n_e(t) - n_e^*(t)|/n_e^*(t)$, averaged within bins of 25 km in altitude h and 5° in SZA, computed using all available relaxation sounding obtained by MAVEN from the middle of January to the end of May 2015. Higher values therefore indicate larger orbit-to-orbit density variation. For reference, we overplot the modeled position of the magnetic pile-up boundary (MPB) as computed by *Edberg et al.* [2008], and the geometric location of the Martian terminator, within this coordinate system. It can be readily seen that the relative variation in density is a minimum at the lowest altitudes sampled on the dayside, in the region of the ionosphere where photochemistry plays a major role in establishing the equilibrium, the influence of solar wind variations is typically smaller, and day-to-day variations in the ionization rate do not yield large amplitude changes in density. However, at increasing altitudes above ∼400 km, the relative density variation rises, as the transport timescale of plasma becomes comparable to that of photochemical lifetime, and large density structures can form. Similarly, the influence of solar wind variations on the structure of the upper ionosphere, causing large motions of the MPB on a range of timescales leads to enhanced variability at higher altitudes. A relatively sharp gradient is noted in the density variations at the terminator, which is here well sampled in situ in the ∼130–300 km altitude range for the first time. As can be seen in Figure 3, the absolute density variations rise by a factor of ∼5–10, while the density itself drops by several orders of magnitude across the terminator [e.g., *Němec et al.*, 2011b]. This larger variability on the nightside may be due to the rapid transport across the terminator of dayside plasma or the creation of localized patches of plasma by particle precipitation.

Finally, despite the relatively early stage of the MAVEN mission, it is nevertheless feasible to show initial statistical evidence for the influence of Mars' crustal fields on the ionospheric density variations. In Figure 4 we simply bin all computed values of the (signed) density variations $\Delta n_e/n_e^* = (n_e - n_e^*)/n_e^*$ which were obtained on the dayside below the nominal MPB in bins of latitude and longitude (5 by 5°). This corresponds
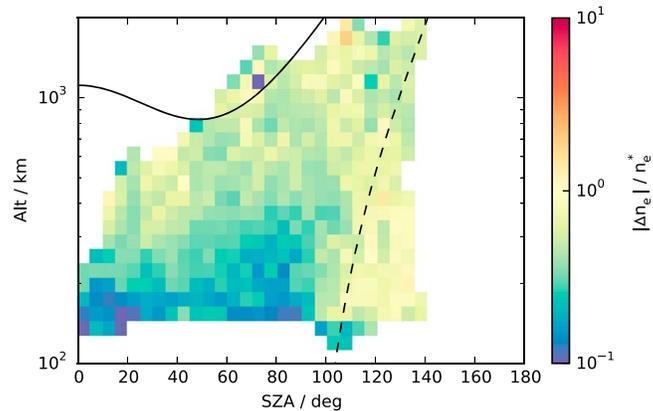
Figure 3. Absolute scaled density deviations $|\Delta n_e/n_e^*| = |n_e - n_e^*|/n_e^*$, binned according to SZA and altitude h. The mean value is shown color coded in each bin. The solid black line indicates the modeled magnetic pile-up boundary altitude according to the model of *Edberg et al.* [2008], while the dashed line shows the geometric terminator of Mars (the area to the right being in shadow).

to all measurements made thus far when MAVEN was located between the solid and dashed lines shown in Figure 3. Contours of the [*Cain et al.*, 2003] field model at 400 km altitude are overplotted at values of $|B| = 50$, 100, and 500 nT (dotted, solid, and dashed lines, respectively). Despite the limited coverage and the relatively poor statistics (65% of bins having less than 100 independent measurements within them), we nevertheless tentatively suggest that the generally positive (red) values of $\Delta n_e/n_e^*$ seen in the stronger field regions in the southern hemisphere are evidence of a systematic effect. The quantity $\Delta n_e/n_e^*$ can only be on average positive if the typical electron densities n_e are higher in these regions of more intense crustal fields, compared to those others locations which form the "baseline" n_e^* (i.e., obtained on similar trajectories but covering different planetary longitudes). Demonstrating such an effect by directly binning measured values of n_e is challenging given the much larger first-order systematic variations in density with SZA and altitude, and is therefore not possible with this relatively small data set.

The generally positive values of $\Delta n_e/n_e^*$ seen in the stronger field regions in the southern hemisphere are balanced by generally negative values elsewhere in the southern hemisphere, while those variations recorded in the northern hemisphere are typically smaller (approaching a zero mean) and without any significant spatial organization evident. At the highest northern latitudes sampled, the typical absolute values of $\Delta n_e/n_e^*$ are somewhat larger, likely as a result of both poorer coverage at this early stage of the mission and some bias toward measurements made at higher altitudes, where the density variability is typically higher (cf. Figure 3)
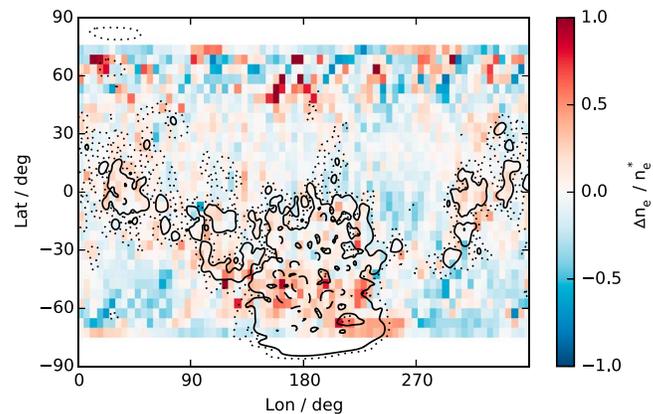
Figure 4. Scaled (signed) density deviations $\Delta n_e/n_e^* = (n_e - n_e^*)/n_e^*$, binned according to planetographic latitude and longitude. Only data taken on the dayside and below the nominal MPB location are included (i.e., all data falling between the solid and dashed lines in Figure 3). Contours of the *Cain et al.* [2003] field model at 400 km altitude for $|B| = 50$, 100, and 500 nT are indicated by the dotted, solid, and dashed black lines, respectively.

3. Summary and Discussion

In this paper we have presented some initial investigations into the structure and variation of the thermal plasma density of the Martian ionosphere, using data obtained by the recently arrived MAVEN mission. Data from the LPW instrument were used to derive plasma densities both using relaxation sounding and measurements of probe-plasma *I-V* sweeps. While further work is required to extract the full potential of this data set, we nevertheless have shown that it is able to measure plasma density variations on short (orbital) timescales with high accuracy. Moreover, we believe this technique to be relatively insensitive to the varying spacecraft potential, which can occasionally strongly disrupt other measurements onboard the spacecraft.

Studying orbit-to-orbit variations, removing (or at least strongly suppressing) the large-scale variations associated with the principal coordinates SZA and *h*, we show that significant plasma density variations are typically recorded at higher altitudes on the dayside and throughout the nightside. The photochemically dominated ionosphere at low altitudes on the dayside is generally more stable, as may be expected — larger energy input here is required to effect a change in its structure. The increase in plasma density variation beyond the terminator indicates the transient, "patchy" nature of the nightside ionosphere. Both transterminator (day to night) plasma flow and local ionization by particle precipitation have been mooted as possibilities for the formation of the nightside ionosphere [e.g., *Shinagawa and Cravens*, 1989; *Fox et al.*, 1993]. The mediation of access of precipitating particles by the crustal fields is clearly compatible with the observed orbit-to-orbit variations in nightside plasma density [*Brain et al.*, 2006; *Lillis et al.*, 2009]. Similarly, deviation of any transterminator plasma flows by the crustal fields, along with the growth of "turbulence" in the accelerating flow can also explain the increased nightside variability and it's rapid increase at the terminator.

Additionally, we have provided initial evidence within the MAVEN LPW data set of the control exerted over the Martian ionosphere by the planet's intense and varied crustal magnetic fields. We find evidence that the enhanced plasma densities over regions of relatively stronger crustal fields seen on the dayside in in situ measurements made by both the MARSIS and Analyzer of Space Plasmas and Energetic Atoms 3 instruments onboard MEX is present at all altitudes down to (approximately) the peak of the ionosphere and certainly into the region in which photochemistry is dominant over transport processes [*Andrews et al.*, 2013, 2015; *Dubinin et al.*, 2012; *Lundin et al.*, 2011; *Nilsson et al.*, 2011]. Future studies will exploit data from this and other MAVEN instruments in studying this control in detail.

References

Acuña, M., et al. (1998), Magnetic field and plasma observations at Mars: Initial results of the Mars global surveyor mission, *Science*, *279*(5357), 1676–1680.

Andersson, L., R. E. Ergun, G. T. Delory, A. I. Eriksson, J. Westfall, H. Reed, J. McCauly, D. Summers, and D. Meyers (2015), The Langmuir Probe and Waves instrument for MAVEN, *Space Sci. Rev.*, doi:10.1007/s11214-015-0194-3, in press.

Andrews, D. J., H. J. Opgenoorth, N. J. T. Edberg, M. André, M. Fränz, E. Dubinin, F. Duru, D. Morgan, and O. Witasse (2013), Determination of local plasma densities with the MARSIS radar: Asymmetries in the high-altitude Martian ionosphere, *J. Geophys. Res. Space Physics*, *118*, 6228–6242, doi:10.1002/jgra.50593.

Andrews, D. J., M. André, H. J. Opgenoorth, N. J. T. Edberg, C. Diéval, F. Duru, D. A. Gurnett, D. Morgan, and O. Witasse (2014), Oblique reflections in the Mars Express MARSIS data set: Stable density structures in the Martian ionosphere, *J. Geophys. Res. Space Physics*, *119*, 3944–3960, doi:10.1002/2013JA019697.

Andrews, D. J., N. J. T. Edberg, A. I. Eriksson, D. A. Gurnett, D. Morgan, F. Němec, and H. J. Opgenoorth (2015), Control of the topside Martian ionosphere by crustal magnetic fields, *J. Geophys. Res. Space Physics*, *120*, 3042–3058, doi:10.1002/2014JA020703.

Barabash, S., et al. (2006), The Analyzer of Space Plasmas and Energetic Atoms (ASPERA-3) for the Mars express mission, *Space Sci. Rev.*, *126*, 113–164, doi:10.1007/s11214-006-9124-8.

Boehm, M. H., C. W. Carlson, J. P. McFadden, J. H. Clemmons, R. E. Ergun, and F. S. Mozer (1994), Wave rectification in plasma sheaths surrounding electric field antennas, *J. Geophys. Res.*, *99*(A11), 21,361–21,374.

Brain, D. A., F. Bagenal, M. H. Acuña, and J. E. P. Connerney (2003), Martian magnetic morphology: Contributions from the solar wind and crust, *J. Geophys. Res.*, *108*, 1424, doi:10.1029/2002JA009482.

Brain, D. A., J. S. Halekas, R. Lillis, D. L. Mitchell, R. P. Lin, and D. H. Crider (2005), Variability of the altitude of the Martian sheath, *Geophys. Res. Lett.*, *321*, L18203, doi:10.1029/2005GL023126.

Brain, D. A., D. L. Mitchell, and J. S. Halekas (2006), The magnetic field draping direction at Mars from April 1999 through August 2004, *Icarus*, *182*, 464–473, doi:10.1016/j.icarus.2005.09.023.

Cain, J. C., B. B. Ferguson, and D. Mozzoni (2003), An n = 90 internal potential function of the Martian crustal magnetic field, *J. Geophys. Res.*, *108*, 5008, doi:10.1029/2000JE001487.

Cartacci, M., E. Amata, A. Cicchetti, R. Noschese, S. Giuppi, B. Langlais, A. Frigeri, R. Orosei, and G. Picardi (2013), Mars ionosphere total electron content analysis from MARSIS subsurface data, *Icarus*, *223*, 423–437, doi:10.1016/j.icarus.2012.12.011.

Dubinin, E., M. Fränz, J. Woch, G. Chanteur, F. Duru, D. A. Gurnett, S. Barabash, and R. Lundin (2012), Upper atmosphere of Mars is not axially symmetrical, *Earth Planets Space*, *64*, 113–120, doi:10.5047/eps.2011.05.022.

Duru, F., D. A. Gurnett, T. F. Averkamp, D. L. Kirchner, R. L. Huff, A. M. Persoon, J. J. Plaut, and G. Picardi (2006), Magnetically controlled structures in the ionosphere of Mars, *J. Geophys. Res.*, *111*, A12204, doi:10.1029/2006JA011975.

Duru, F., D. A. Gurnett, R. A. Frahm, J. D. Winningham, D. D. Morgan, and G. G. Howes (2009), Steep, transient density gradients in the Martian ionosphere similar to the ionopause at Venus, *J. Geophys. Res.*, *114*, A12310, doi:10.1029/2009JA014711.

Duru, F., D. A. Gurnett, D. D. Morgan, J. D. Winningham, R. A. Frahm, and A. F. Nagy (2011), Nightside ionosphere of Mars studied with local electron densities: A general overview and electron density depressions, *J. Geophys. Res.*, *116*, A10316, doi:10.1029/2011JA016835.

Edberg, N. J. T., M. Lester, S. W. H. Cowley, and A. I. Eriksson (2008), Statistical analysis of the location of the Martian magnetic pileup boundary and bow shock and the influence of crustal magnetic fields, *J. Geophys. Res.*, *113*, A08206, doi:10.1029/2008JA013096.

Ergun, R. E., et al. (2008), Eigenmode structure in solar-wind Langmuir waves, *Phys. Rev. Lett.*, *101*(5), 51,101, doi:10.1103/PhysRevLett.101.051101.

Ergun, R. E., M. W. Morooka, L. A. Andersson, C. M. Fowler, G. T. Delory, D. J. Andrews, A. I. Eriksson, T. McEnulty, and B. M. Jakosky (2015), Dayside electron temperature and density profiles at Mars: First results from the MAVEN Langmuir probe and waves instrument, *Geophys. Res. Lett.*, *42*, doi:10.1002/2015GL065280.

Fowler, C. M., et al. (2015), The first in situ electron temperature and density measurements of the Martian nightside ionosphere, *Geophys. Res. Lett.*, *42*, doi:10.1002/2015GL065267.

Fox, J. L., J. F. Brannon, and H. S. Porter (1993), Upper limits to the nightside ionosphere of Mars, *Geophys. Res. Lett.*, *20*(13), 1339–1342, doi:10.1029/93GL01349.

Gurnett, D. A., D. L. Kirchner, R. L. Huff, D. D. Morgan, A. M. Persoon, T. F. Averkamp, F. Duru, E. Nielsen, A. Safaeinili, J. J. Plaut, and G. Picardi (2005), Radar soundings of the ionosphere of Mars, *Science*, *310*, 1929–1933, doi:10.1126/science.1121868.

Gurnett, D. A., D. D. Morgan, F. Duru, F. Akalin, J. D. Winningham, R. A. Frahm, E. Dubinin, and S. Barabash (2010), Large density fluctuations in the Martian ionosphere as observed by the Mars Express radar sounder, *Icarus*, *206*, 83–94, doi:10.1016/j.icarus.2009.02.019.

Hanson, W. B., S. Sanatani, and D. R. Zuccaro (1977), The Martian ionosphere as observed by the Viking retarding potential analyzers, *J. Geophys. Res.*, *82*, 4351–4363, doi:10.1029/JS082i028p04351.

Jakosky, B., et al. (2015), The Mars Atmosphere and Volatile Evolution (MAVEN) Mission, *Space Sci. Rev.*, 1–46, doi:10.1007/s11214-015-0139-x.

Kliore, A. J. (1992), Radio occultation observations of the ionospheres of Mars and Venus, in *Venus and Mars: Atmospheres, Ionosphere and Solar Wind Interactions, Geophys. Monogr. Ser.*, vol. 66, pp. 265–276, AGU, Washington, D. C.

Kolesnikova, E., C. Béghin, R. Grard, and C. P. Escoubet (2001), The electrical stability of the electric field antennas in the plasmasphere, *J. Atmos. Terr. Phys.*, *63*, 1217–1224.

Lillis, R. J., and D. A. Brain (2013), Nightside electron precipitation at Mars: Geographic variability and dependence on solar wind conditions, *J. Geophys. Res. Space Physics*, *118*, 3546–3556, doi:10.1002/jgra.50171.

Lillis, R. J., M. O. Fillingim, L. M. Peticolas, D. A. Brain, R. P. Lin, and S. W. Bougher (2009), Nightside ionosphere of Mars: Modeling the effects of crustal magnetic fields and electron pitch angle distributions on electron impact ionization, *J. Geophys. Res.*, *114*, E11009, doi:10.1029/2009JE003379.

Lundin, R., S. Barabash, M. Yamauchi, H. Nilsson, and D. Brain (2011), On the relation between plasma escape and the Martian crustal magnetic field, *Geophys. Res. Lett.*, *38*, L02102, doi:10.1029/2010GL046019.

Mendillo, M., C. Narvaez, P. Withers, M. Matta, W. Kofman, and J. Mouginot (2013), Variability in ionospheric total electron content at Mars, *Planet. Space. Sci.*, *86*, 117–129, doi:10.1016/j.pss.2013.08.010.

Mitchell, D. L., R. P. Lin, C. Mazelle, H. Rème, P. A. Cloutier, J. E. P. Connerney, M. H. Acuña, and N. F. Ness (2001), Probing Mars' crustal magnetic field and ionosphere with the MGS Electron Reflectometer, *J. Geophys. Res.*, *106*, 23,419–23,428, doi:10.1029/2000JE001435.

Nagy, A. F., et al. (2004), The plasma environment of Mars, *Space Sci. Rev.*, *111*, 33–114, doi:10.1023/B:SPAC.0000032718.47512.92.

Nilsson, H., N. J. T. Edberg, G. Stenberg, S. Barabash, M. Holmström, Y. Futaana, R. Lundin, and A. Fedorov (2011), Heavy ion escape from Mars, influence from solar wind conditions and crustal magnetic fields, *Icarus*, *215*, 475–484, doi:10.1016/j.icarus.2011.08.003.

Němec, F., D. D. Morgan, D. A. Gurnett, and F. Duru (2010), Nightside ionosphere of Mars: Radar soundings by the Mars Express spacecraft, *J. Geophys. Res.*, *115*, E12009, doi:10.1029/2010JE003663.

Němec, F., D. D. Morgan, D. A. Gurnett, and D. A. Brain (2011a), Areas of enhanced ionization in the deep nightside ionosphere of Mars, *J. Geophys. Res.*, *116*, E06006, doi:10.1029/2011JE003804.

Němec, F., D. D. Morgan, D. A. Gurnett, F. Duru, and V. Truhlík (2011b), Dayside ionosphere of Mars: Empirical model based on data from the MARSIS instrument, *J. Geophys. Res.*, *116*, E07003, doi:10.1029/2010JE003789.

Němec, F., D. D. Morgan, C. Diéval, D. A. Gurnett, and Y. Futaana (2014), Enhanced ionization of the martian nightside ionosphere during solar energetic particle events, *Geophys. Res. Lett.*, *41*, 793–798, doi:10.1002/2013GL058895.

Pätzold, M., et al. (2004), MaRS: Mars express orbiter radio science, in *Mars Express: The Scientific Payload*, vol. 1240, edited by A. Wilson and A. Chicarro, pp. 141–163, ESA Special Publ., Noordwijk, Netherlands.

Picardi, G., et al. (2004), MARSIS: Mars advanced radar for subsurface and ionosphere sounding, in *Mars Express: The Scientific Payload*, vol. 1240, edited by A. Wilson and A. Chicarro, pp. 51–69, ESA Special Publ., Noordwijk, Netherlands.

Shinagawa, H., and T. E. Cravens (1989), A one-dimensional multispecies magnetohydrodynamic model of the dayside ionosphere of Mars, *J. Geophys. Res.*, *94*, 6506–6516, doi:10.1029/JA094iA06p06506.

Tyler, G. L., G. Balmino, D. P. Hinson, W. L. Sjogren, D. E. Smith, R. A. Simpson, S. W. Asmar, P. Priest, and J. D. Twicken (2001), Radio science observations with Mars Global Surveyor: Orbit insertion through one Mars year in mapping orbit, *J. Geophys. Res.*, *106*, 23,327–23,348, doi:10.1029/2000JE001348.

Witasse, O., T. Cravens, M. Mendillo, J. Moses, A. Kliore, A. Nagy, and T. Breus (2008), Solar system ionospheres, *Space Sci. Rev.*, *139*, 235–265, doi:10.1007/s11214-008-9395-3.

Withers, P. (2009), A review of observed variability in the dayside ionosphere of Mars, *Adv. Space Res.*, *44*, 277–307, doi:10.1016/j.asr.2009.04.027.

Zhang, M. H. G., J. G. Luhmann, and A. J. Kliore (1990), An observational study of the nightside ionospheres of Mars and Venus with radio occultation methods, *J. Geophys. Res.*, *95*, 17,095–17,102, doi:10.1029/JA095iA10p17095.